Electron acceleration caused by small pulses in shock waves

Masatoshi Sato, Seiji Miyahara, and Yukiharu Ohsawa[a)]
Department of Physics, Nagoya University, Nagoya 464-8602, Japan

(Received 22 November 2004; accepted 22 February 2005; published online 22 April 2005)

A new particle acceleration mechanism is studied with theory and particle simulations. Around small pulses that are generated in a large-amplitude shock wave in a magnetized plasma, electrons can be accelerated to ultrarelativistic energies. Simulations demonstrate electron acceleration to energies $\gamma > 100$ in weak magnetic fields such that $|\Omega_e|/\omega_{pe} < 1$ as well as in strong magnetic fields. The theoretical model accounts for the basic features of the electron motion in the simulations. © *2005 American Institute of Physics*. [DOI: 10.1063/1.1895885]

I. INTRODUCTION

Electron acceleration to ultrarelativistic energies in an oblique shock wave has recently been found with particle simulations.[1–3] Electrons can be reflected in the end of the main pulse of the shock wave. The reflection takes place when a negative dip of F is formed there, where $F=\int E_{\parallel} ds$ with $E_{\parallel}$ being the electric field parallel to the magnetic field $\boldsymbol{B}$ and ds the infinitesimal length along $\boldsymbol{B}$. Negative dips are generated in association with nonstationary behavior of the wave. These reflected electrons are then trapped and have very high energies near the position at which the magnetic field has its maximum value. For a shock wave propagating in the x direction with a speed v_{sh} in an external magnetic field $\boldsymbol{B}_0=(B_{x0},0,B_{z0})$, the maximum energy of accelerated electrons is given by

$$K_w = \frac{e\phi_w}{1-(v_{sh}/c)(B_{wz0}/B_{wx0})}, \tag{1}$$

where ϕ is the magnitude of the electric potential formed in the shock wave, c is the speed of light, and the subscript w refers to quantities in the wave frame. This indicates that K can have extremely great values when $1-(v_{sh}/c)\times(B_{wz0}/B_{wx0})\sim 0$. In terms of the quantities in the laboratory frame, this is expressed as

$$v_{sh} \sim c\cos\theta, \tag{2}$$

where θ is the shock propagation angle, $\tan\theta = B_{z0}/B_{x0}$. Particle simulations have demonstrated electron acceleration to Lorentz factors γ greater than 100 in a rather strong magnetic field such that $|\Omega_e|/\omega_{pe} \gtrsim 1$, where $|\Omega_e|$ and ω_{pe} are the electron gyrofrequency and plasma frequency in the upstream region, respectively. The present mechanism will be important, for instance, in solar magnetic tubes[4,5] and around pulsars[6,7] where the magnetic fields are strong.

It is also quite interesting and important to explore electron acceleration mechanisms in weak magnetic fields. In fact, it has been reported that electrons are accelerated to very high energies in the shock wave of supernova remnant SN1006, where the magnetic field is thought to be quite weak.[8,9]

In this paper, we study electron acceleration that works in weak magnetic fields as well as in strong magnetic fields. It is found that such a mechanism does exist in large-amplitude shock waves. Strong electron acceleration can occur immediately behind small pulses generated in nonstationary shock waves.

In Sec. II, we theoretically discuss this mechanism. We analyze electron motions inside and outside a small pulse and obtain the amount of energy that these electrons can gain. In a nonstationary shock wave, small-amplitude pulses are generated. They propagate with speeds slightly lower than the main pulse of the shock wave. The speeds of these pulses relative to the background medium around them are quite small, because the medium is also moving in the shock region. Some particles therefore can stay around small pulses for long periods of time and can gain a great amount of energy from the electric field. In a large area behind the shock front, there exist electric and magnetic fields. Hence, electric fields are present inside and outside the small pulse. Electrons obtain energy mainly from the electric field behind the small pulse. In Sec. III, we perform one-dimensional (one space coordinate and three velocities) electromagnetic particle simulations and show that electrons can be accelerated to ultrarelativistic energies with $\gamma > 100$ in a shock wave with this mechanism. An interesting feature of this mechanism is that the region where the acceleration takes place slowly moves away from the shock front to the downstream region, which results from the fact that the propagation speeds of the small pulses are slightly lower than that of the main pulse. The present mechanism works when the external magnetic field is either weak, $|\Omega_e|/\omega_{pe} < 1$, or strong. Also, it does not require the condition (2). We summarize our work in Sec. IV.

II. THEORY OF ELECTRON ACCELERATION

A. Perpendicular pulse

First, we analytically discuss the electron acceleration in a perpendicular wave. Oblique waves will be discussed in Sec. II G. We consider a shock wave propagating in the x direction with a velocity $v_{sh}(>0)$ in an external magnetic field

[a)]Electronic mail: ohsawa@nagoya-u.jp

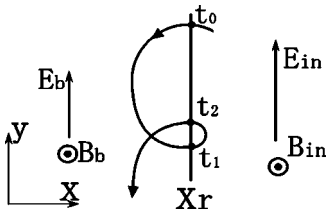

FIG. 1. Electric and magnetic fields in and behind a small pulse. Schematic orbit of an electron crossing the rear edge of the pulse, $x=x_r$, is also shown.

$$\boldsymbol{B}_0 = (0,0,B_{z0}). \tag{3}$$

For definiteness, we assume that $B_{z0}>0$. In the laboratory frame, the electric field E_y formed in the shock wave is positive.[10–15] Macroscopic electric fields do not exist in the upstream region. The x component of the $\boldsymbol{E}\times\boldsymbol{B}$ drift velocity is

$$v_{dx}(x) = c\frac{E_y(x)}{B_z(x)}. \tag{4}$$

Since E_y and B_z are both positive, v_{dx} is also positive. Faraday's law gives

$$E_y(x) = \frac{v_{\rm sh}}{c}[B_z(x) - B_{z0}] \tag{5}$$

for a stationary wave. Equation (4) can then be written as

$$v_{dx}(x) = v_{\rm sh}\left(1 - \frac{B_{z0}}{B_z(x)}\right). \tag{6}$$

Since B_z in the shock wave is greater than B_{z0}, v_{dx} is in the range $0<v_{dx}<v_{\rm sh}$; electron positions move to the downstream region of the shock wave.

The propagation of large-amplitude shock waves is not perfectly stationary.[1,16,17] For instance, nonstationary behavior of a shock wave created by the ion reflection has been discussed in detail in Ref. 17. Owing to such nonstationary behavior, small-amplitude pulses can be produced behind the front of a large-amplitude shock wave.[1,17] As will be shown with particle simulations later in Sec. III, some of them move with a velocity $v_{\rm sh2}$ close to the drift speed,

$$v_{\rm sh2} \sim v_{dx}. \tag{7}$$

In the following, we develop an electron acceleration theory assuming Eq. (7).

In the discussion of electron motion, we assume, for simplicity, that the shape of the small pulse is rectangular with a width Δ. Hence, in the pulse region

$$x_r < x < x_r + \Delta, \tag{8}$$

where x_r is the rear edge of the small pulse, the electric and magnetic fields are constant and are given as

$$\boldsymbol{E}_{\rm in} = (0,E_{\rm in},0), \tag{9}$$

$$\boldsymbol{B}_{\rm in} = (0,0,B_{\rm in}) \tag{10}$$

(see Fig. 1). Behind the pulse, $x<x_r$, the fields may be written as

$$\boldsymbol{E}_b = (0,E_b,0), \tag{11}$$

$$\boldsymbol{B}_b = (0,0,B_b). \tag{12}$$

The fields are stronger inside the pulse than outside,

$$E_{\rm in} > E_b, \tag{13}$$

$$B_{\rm in} > B_b. \tag{14}$$

The x component of the electric field E_x will also be present at the boundaries of the pulse.

We discuss motions of electrons that cross the rear edge, $x=x_r$, several times (see Fig. 1).

B. Electron motion inside the small pulse

Inside the small pulse, $x_r<x<x_r+\Delta$, the relativistic equation of motion for electrons reads as

$$m_e\frac{d}{dt}(\gamma v_x) = -\frac{e}{c}v_y B_{\rm in}, \tag{15}$$

$$m_e\frac{d}{dt}(\gamma v_y) = -eE_{\rm in} + \frac{e}{c}v_x B_{\rm in}. \tag{16}$$

The z component of the momentum is constant because $E_z=0$,

$$p_z = \text{const}. \tag{17}$$

From Eqs. (15) and (16), we obtain

$$m_e c^2(\gamma - \gamma_{0\rm in}) = -eE_{\rm in}(y - y_{0\rm in}), \tag{18}$$

where $\gamma_{0\rm in}$, which is defined as

$$\gamma_{0\rm in} = [1 + (p_{x0}^2 + p_{y0}^2 + p_z^2)/(m_e^2c^2)]^{1/2}, \tag{19}$$

and $y_{0\rm in}$ are constant. Integrating Eq. (15), we find

$$m_e\gamma v_x - m_e\gamma_{0\rm in}v_{x0\rm in} = -\frac{eB_{\rm in}}{c}(y - y_{0\rm in}). \tag{20}$$

Combining Eqs. (18) and (20), and using the relation $\gamma=[1+\boldsymbol{p}^2/(m_e^2c^2)]^{1/2}$, we obtain an elliptic equation for $\boldsymbol{p}$,

$$\frac{(p_x - P_{\rm in})^2}{a_{\rm in}^2} + \frac{p_y^2}{(a_{\rm in}/\gamma_{d\rm in})^2} = 1, \tag{21}$$

where $\gamma_{d\rm in}=(1-v_{d\rm in}^2/c^2)^{-1/2}$ with

$$v_{d\rm in} = c\frac{E_{\rm in}}{B_{\rm in}}. \tag{22}$$

Also, $P_{\rm in}$ and $a_{\rm in}$ are defined as

$$P_{\rm in} = m_e\gamma_{d\rm in}^2 v_{d\rm in}\gamma_{0\rm in}(1 - v_{d\rm in}v_{x0\rm in}/c^2), \tag{23}$$

$$a_{\rm in}^2 = (c^2/v_{d\rm in}^2)P_{\rm in}^2 - (m_e^2c^2 + p_z^2)\gamma_{d\rm in}^2. \tag{24}$$

The quantity $P_{\rm in}$ is positive because $v_{d\rm in}>0$. Also, it is proved in Appendix A that $a_{\rm in}^2 \geqslant 0$. We take $a_{\rm in}$ to be positive.

C. Electron motion behind the small pulse

Behind the small pulse, $x<x_r$, electrons also make elliptic motions in the momentum space,

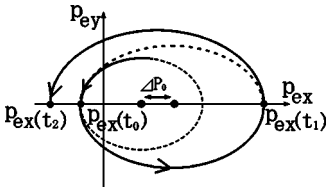

FIG. 2. Change in elliptic motion in the momentum space.

$$\frac{(p_x - P_b)^2}{a_b^2} + \frac{p_y^2}{(a_b/\gamma_{db})^2} = 1, \tag{25}$$

where

$$P_b = m_e \gamma_{db}^2 v_{db} \gamma_{0b}(1 - v_{db} v_{x0b}/c^2), \tag{26}$$

$$a_b^2 = (c^2/v_{db}^2) P_b^2 - (m_e^2 c^2 + p_z^2)\gamma_{db}^2, \tag{27}$$

with

$$v_{db} = c\frac{E_b}{B_b}, \tag{28}$$

and $\gamma_{db}=(1-v_{db}^2/c^2)^{-1/2}$. As in Sec. II B, one can show that

$$P_b \geqslant 0, \tag{29}$$

$$a_b^2 \geqslant 0. \tag{30}$$

We take a_b to be positive.

D. Connection between the motions inside and outside the small pulse

As an electron moves from inside to outside the small pulse, crossing its rear boundary, the elliptic motion in the momentum space continuously changes from the one represented by Eq. (21) to the one by Eq. (25). Also, when the electron returns to the pulse region, the elliptic motion changes again. Some electrons would repeat these processes several times.

We consider an electron that goes out to the outside region crossing the rear boundary $x=x_r$ at $t=t_0$ and, after a half gyration, goes into the pulse at $t=t_1$ (see Fig. 1). Because $E_y>0$, the electron gains energy during this time. It obtains the greatest amount of energy when $p_y(t_0)$ and $p_y(t_1)$ are both zero. That is, for a given initial energy, the shift in the y direction, $|y(t_1)-y(t_0)|$, becomes the largest when $p_y(t_0)=p_y(t_1)=0$. This type of motion can occur when $v_{db}=v_{\mathrm{sh2}}$ (see Appendix B). In the following, the relation $p_y(t_0)\sim p_y(t_1)\sim 0$ is assumed.

Figure 2 shows a schematic electron orbit in the momentum space. When the particle goes out to the region behind the pulse at $t=t_0$ with $p_y(t_0)=0$, the center of the ellipse is shifted along the p_x axis by

$$\Delta P_0 = P_b - P_{\mathrm{in}}. \tag{31}$$

Taking the constants in Eqs. (23) and (26) to be

$$\gamma_{0\mathrm{in}} = \gamma_{0b} = \gamma(t_0), \tag{32}$$

$$v_{x0\mathrm{in}} = v_{x0b} = v_x(t_0), \tag{33}$$

we find ΔP_0 as

$$\Delta P_0 = m_e c \gamma(t_0)(\gamma_{d\mathrm{in}}^2 \beta_{d\mathrm{in}}^2 - \gamma_{db}^2 \beta_{db}^2) \times \left[\frac{v_x(t_0)}{c} - \left(1 + \frac{(1-\beta_{d\mathrm{in}})(1-\beta_{db})}{\beta_{db} + \beta_{d\mathrm{in}}} \right) \right], \tag{34}$$

where $\beta_{d\mathrm{in}}$ and β_{db} are defined as

$$\beta_{d\mathrm{in}} = v_{d\mathrm{in}}/c, \tag{35}$$

$$\beta_{db} = v_{db}/c. \tag{36}$$

It is shown in Appendix C that if the propagation of the small pulse is nearly stationary, the relation

$$v_{db} > v_{d\mathrm{in}} > v_{\mathrm{sh2}} \tag{37}$$

or

$$v_{db} < v_{d\mathrm{in}} < v_{\mathrm{sh2}} \tag{38}$$

must be satisfied. The latter, Eq. (38), is an ordinary relation for nonlinear pulses propagating in an equilibrium plasma.[10–15] In the present situation, the small pulse is in a large-amplitude shock wave and is propagating with a slightly lower speed than the shock wave. Hence, we here assume the former relation, Eq. (37), with the speeds v_{db}, $v_{d\mathrm{in}}$, and v_{sh2} being very close. Then, since the relation

$$\gamma_{d\mathrm{in}}^2 \beta_{d\mathrm{in}}^2 - \gamma_{db}^2 \beta_{db}^2 < 0 \tag{39}$$

holds, we find that the shift is positive,

$$\Delta P_0 > 0. \tag{40}$$

In the same way, we obtain the shift of the ellipse center at $t=t_1$ as

$$\Delta P_1 = P_{\mathrm{in}} - P_b = m_e c \gamma(t_1)(\gamma_{db}^2 \beta_{db}^2 - \gamma_{d\mathrm{in}}^2 \beta_{d\mathrm{in}}^2) \times \left[\frac{v_x(t_1)}{c} - \left(1 + \frac{(1-\beta_{db})(1-\beta_{d\mathrm{in}})}{\beta_{d\mathrm{in}} + \beta_{db}} \right) \right]. \tag{41}$$

Under the condition (37), this is negative

$$\Delta P_1 < 0. \tag{42}$$

E. Energy change

We now discuss the energy change in these elliptic motions. If we know the momentum $p_x(t_0)$, then by substituting it in Eqs. (26) and (27), we obtain the momentum at $t=t_1$,

$$p_x(t_1) = P_b[p_x(t_0)] + a_b[p_x(t_0)]. \tag{43}$$

Similarly, using $p_x(t_1)$, we find the momentum at $t=t_2$ as

$$p_x(t_2) = P_{\mathrm{in}}[p_x(t_1)] - a_{\mathrm{in}}[p_x(t_1)]. \tag{44}$$

In this way, we can successively obtain the momentum at the lth crossing ($l=1,2,3,\ldots$) from the initial $p_x(t_0)$. When $l=2n$ with n an integer, i.e., when the particle goes out from the small pulse to the downstream region, $p_x(t_{2n})$ is negative and is given as

$$p_x(t_{2n}) = P_{\rm in}[p_x(t_{2n-1})] - a_{\rm in}[p_x(t_{2n-1})]. \tag{45}$$

When $l=2n+1$, i.e., when the particle goes into the small pulse from the downstream region, $p_x(t_{2n+1})$ is positive,

$$p_x(t_{2n+1}) = P_b[p_x(t_{2n})] + a_b[p_x(t_{2n})]. \tag{46}$$

For $\gamma \gg 1$ with

$$\gamma(t_{2n}) \sim -p_x(t_{2n})/(m_e c), \tag{47}$$

i.e., $p_x(t_{2n})$ is much greater than p_y and p_z in magnitude, we have

$$a_b^2 \sim (c^2/v_{db}^2)P_b^2, \tag{48}$$

$$P_b \sim m_e \gamma_{db}^2 v_{db} \gamma(t_{2n})(1 + v_{db}/c). \tag{49}$$

We therefore have

$$\gamma(t_{2n+1}) \sim \gamma_{db}^2 \frac{v_{db}}{c}\left(1 + \frac{v_{db}}{c}\right)\left(1 + \frac{c}{v_{db}}\right)\gamma(t_{2n}). \tag{50}$$

On account of the relation $\gamma_{db}^2 = (1 - v_{db}^2/c^2)^{-1}$, Eq. (50) can be further simplified as

$$\gamma(t_{2n+1}) \sim \frac{1 + E_b/B_b}{1 - E_b/B_b}\gamma(t_{2n}). \tag{51}$$

The ratio $\gamma(t_{2n+1})/\gamma(t_{2n})$ is independent of n, only dependent on the ratio E_b/B_b. If E_b/B_b is close to unity behind the small pulse, the energy enhancement should be significant.

In the same way, under the assumption

$$\gamma(t_{2n-1}) \sim p_x(t_{2n-1})/(m_e c), \tag{52}$$

we find that

$$a_{\rm in}^2 \sim (c^2/v_{d\rm in}^2)P_{\rm in}^2, \tag{53}$$

$$P_{\rm in} \sim m_e \gamma_{d\rm in}^2 v_{d\rm in} \gamma(t_{2n-1})(1 - v_{d\rm in}/c). \tag{54}$$

It then follows that

$$\gamma(t_{2n}) \sim \gamma_{d\rm in}^2 \frac{v_{d\rm in}}{c}\left(1 - \frac{v_{d\rm in}}{c}\right)\left(-1 + \frac{c}{v_{d\rm in}}\right)\gamma(t_{2n-1}), \tag{55}$$

which can be simplified as

$$\gamma(t_{2n}) \sim \frac{1 - E_{\rm in}/B_{\rm in}}{1 + E_{\rm in}/B_{\rm in}}\gamma(t_{2n-1}). \tag{56}$$

F. Energy increase rate

The energy takes its maxima at $t=t_{2n+1}$ and minima at $t=t_{2n}$. We calculate the increase rate of the maxima and that of the minima. For an odd number $2n+1$, the time period $t_{2n+1}-t_{2n}$ is calculated as

$$t_{2n+1} - t_{2n} = \gamma_{db}^3\left(\gamma(t_{2n}) - \frac{v_{db}}{c}\frac{p_x(t_{2n})}{m_e c}\right)\frac{\pi}{|\Omega_{eb}|}, \tag{57}$$

where $|\Omega_{eb}|$ is the nonrelativistic electron gyrofrequency in the region behind the small pulse (see Appendix B). For an even number $2n$, the time period is

$$t_{2n} - t_{2n-1} = \gamma_{d\rm in}^3\left(\gamma(t_{2n-1}) - \frac{v_{d\rm in}}{c}\frac{p_x(t_{2n-1})}{m_e c}\right)\frac{\pi}{|\Omega_{e\rm in}|}. \tag{58}$$

For large γ, they become

$$t_{2n+1} - t_{2n} \sim \frac{\gamma_{db}}{(1 - E_b/B_b)}\frac{\pi}{|\Omega_{eb}|}\gamma(t_{2n}), \tag{59}$$

$$t_{2n} - t_{2n-1} \sim \frac{\gamma_{d\rm in}}{(1 + E_{\rm in}/B_{\rm in})}\frac{\pi}{|\Omega_{e\rm in}|}\gamma(t_{2n-1}). \tag{60}$$

The particle spends much longer time in the region behind the small pulse than in the small pulse,

$$t_{2n+1} - t_{2n} > t_{2n} - t_{2n-1}. \tag{61}$$

From these relations, we can estimate the increase rate of the peak values of γ, $[\gamma(t_{2n+1}) - \gamma(t_{2n-1})]/(t_{2n+1} - t_{2n-1})$. From Eqs. (51) and (56), it follows that

$$\gamma(t_{2n+1}) - \gamma(t_{2n-1}) = \left[\left(\frac{1 + E_b/B_b}{1 - E_b/B_b}\right)\left(\frac{1 - E_{\rm in}/B_{\rm in}}{1 + E_{\rm in}/B_{\rm in}}\right) - 1\right] \times \gamma(t_{2n-1}). \tag{62}$$

Also, from Eqs. (59) and (60), we have

$$t_{2n+1} - t_{2n-1} = \left(\frac{\gamma_{db}(1 - E_{\rm in}/B_{\rm in})}{(1 - E_b/B_b)(1 + E_{\rm in}/B_{\rm in})} + \frac{\gamma_{d\rm in}}{(1 + E_{\rm in}/B_{\rm in})}\frac{B_b}{B_{\rm in}}\right)\frac{\pi}{|\Omega_{eb}|}\gamma(t_{2n-1}). \tag{63}$$

We therefore find the average time rate of change of the maxima as

$$\frac{d\gamma}{dt} = \frac{\gamma(t_{2n+1}) - \gamma(t_{2n-1})}{t_{2n+1} - t_{2n-1}} \simeq \frac{2|\Omega_{eb}|}{\pi}\frac{(E_b/B_b - E_{\rm in}/B_{\rm in})}{[\gamma_{db}(1 - E_{\rm in}/B_{\rm in}) + \gamma_{d\rm in}(B_b/B_{\rm in})(1 - E_b/B_b)]}. \tag{64}$$

Similarly, we obtain the average time rate of change of the minima

$$\frac{d\gamma}{dt} = \frac{\gamma(t_{2n}) - \gamma(t_{2n-2})}{t_{2n} - t_{2n-2}} \simeq \frac{2|\Omega_{eb}|}{\pi}\frac{(E_b/B_b - E_{\rm in}/B_{\rm in})}{[\gamma_{db}(1 + E_{\rm in}/B_{\rm in}) + \gamma_{d\rm in}(B_b/B_{\rm in})(1 + E_b/B_b)]}. \tag{65}$$

Equations (64) and (65) are both independent of n. The increase rate of the maxima is greater than that of the minima.

G. Oblique waves

For an oblique pulse, we have a constant magnetic field B_{x0} in addition to B_z. We may write the magnetic field in the small pulse as

$$\boldsymbol{B}_{\rm in} = (B_{x0}, 0, B_{\rm inz}), \tag{66}$$

and that behind the pulse as

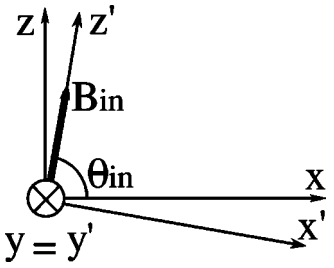

FIG. 3. Coordinate systems (x,y,z) and (x',y',z'). The z' axis is parallel to $\boldsymbol{B}_{\rm in}$.

$$\boldsymbol{B}_b = (B_{x0}, 0, B_{bz}). \tag{67}$$

Here, B_y is neglected. It could be comparable to B_z in large-amplitude shock front. Behind the shock front, however, it should be weak because it is proportional to $\partial B_z/\partial x$.[14,15] The electric fields are taken to be $\boldsymbol{E}_{\rm in}=(0,E_{\rm in},0)$ and $\boldsymbol{E}_b=(0,E_b,0)$. Because the electric field parallel to the magnetic field is weak in magnetohydrodynamic waves, E_y is the dominant component. Hence, the parallel momentum is assumed to be constant in each region. The motion perpendicular to $\boldsymbol{B}$ will then be elliptic in the momentum space.

We introduce a new coordinate system (x',y',z'), where the y' axis is parallel to the y axis and the z' axis is parallel to $\boldsymbol{B}_{\rm in}$ (see Fig. 3). In this coordinate system, the particle motion in the momentum space can be written as

$$\frac{(p_x'-P_{\rm in}')^2}{a_{\rm in}'^2}+\frac{p_y'^2}{(a_{\rm in}'/\gamma_{d\rm in}')^2}=1, \tag{68}$$

where

$$v_{d\rm in}'=c\frac{E_{\rm in}}{B_{\rm in}}, \tag{69}$$

$$P_{\rm in}'=m_e\gamma_{d\rm in}'^2 v_{d\rm in}'\gamma_{0\rm in}(1-v_{d\rm in}'v_{x0\rm in}'/c^2), \tag{70}$$

$$a_{\rm in}'^2=(c^2/v_{d\rm in}'^2)P_{\rm in}'^2-(m_e^2c^2+p_z'^2)\gamma_{d\rm in}'^2. \tag{71}$$

Also, in the coordinate system (x'',y'',z''), where the y'' and z'' axes are parallel to the y axis and to $\boldsymbol{B}_b$, respectively, the particle motion is given as

$$\frac{(p_x''-P_b'')^2}{a_b''^2}+\frac{p_y''^2}{(a_b''/\gamma_{db}'')^2}=1, \tag{72}$$

where

$$v_{db}''=c\frac{E_b}{B_b}, \tag{73}$$

$$P_b''=m_e\gamma_{db}''^2 v_{db}''\gamma_{0b}(1-v_{db}''v_{x0b}''/c^2), \tag{74}$$

$$a_b''^2=(c^2/v_{db}''^2)P_b''^2-(m_e^2c^2+p_z''^2)\gamma_{db}''^2. \tag{75}$$

At the moment $t=t_0$, when a particle crosses the boundary between the regions in and behind the small pulse, the velocities in these regions are related through

$$v_x''=v_x'\cos(\theta_{\rm in}-\theta_b)-v_z'\sin(\theta_{\rm in}-\theta_b), \tag{76}$$

$$v_y''=v_y', \tag{77}$$

$$v_z''=v_x'\sin(\theta_{\rm in}-\theta_b)+v_z'\cos(\theta_{\rm in}-\theta_b). \tag{78}$$

For particles with

$$v_{db}''\cos[(\pi/2)-\theta_b]+v_z''\cos\theta_b\simeq v_{\rm sh2}, \tag{79}$$

the x component of the guiding center velocity is nearly equal to $v_{\rm sh2}$ in the region behind the small pulse. These particles can have the momentum $p_y\simeq 0$ at both $t=t_0$ and $t=t_1$. Substituting Eq. (78) in Eq. (79) yields

$$v_z'(t_0)=\frac{1}{\cos(\theta_{\rm in}-\theta_b)}\left(\frac{v_{\rm sh2}-v_{db}''\sin\theta_b}{\cos\theta_b}-v_x'(t_0)\sin(\theta_{\rm in}-\theta_b)\right). \tag{80}$$

From Eq. (76), then, we find $v_x''(t_0)$ as a function of $v_x'(t_0)$

$$v_x''(t_0)=\frac{v_x'(t_0)}{\cos(\theta_{\rm in}-\theta_b)}-\frac{(v_{\rm sh2}-v_{db}''\sin\theta_b)}{\cos\theta_b}\tan(\theta_{\rm in}-\theta_b). \tag{81}$$

Since $v_{x0\rm in}'=v_x'(t_0)$, $v_{x0b}'=v_x''(t_0)$, and $\gamma_{0b}=\gamma_{0\rm in}$, the quantities P_b'' and a_b'' are given as functions of $v_x'(t_0)$ and $\gamma(t_0)$; we thus obtain the momentum at $t=t_1$,

$$p_x''(t_1)=P_b''[p_x'(t_0)]+a_b''[p_x'(t_0)]. \tag{82}$$

Hence, we have results similar to those in Sec. II E and II F. For large γ, for instance, the maximum energy gain is given as

$$\gamma(t_{2n+1})\sim\frac{1+E_b/B_b}{1-E_b/B_b}\gamma(t_{2n}), \tag{83}$$

which is the same form as Eq. (51). The energy difference $\gamma(t_{2n+1})-\gamma(t_{2n-1})$ and average time rate of change of the maxima are given by Eqs. (62) and (64), respectively. One can use Eq. (65) for the average time rate of change of the minima.

In Appendix C, it is shown that the relation $v_{dbx}>v_{d\rm in x}>v_{\rm sh2}$ or $v_{dbx}<v_{d\rm in x}<v_{\rm sh2}$ must hold. Here, the latter is assumed. Hence, particles satisfying the relation (79) can exist.

We also note that, when an electron crosses the rear boundary of the small pulse, its parallel momentum always decreases. With calculations similar to those in Ref. 18, we obtain the change in the parallel momentum, $\delta p_\parallel=[\boldsymbol{p}(t_1)-\boldsymbol{p}(t_0)]\cdot\boldsymbol{B}_{\rm in}$ as

$$\delta p_\parallel=[p_x''(t_1)-p_x''(t_0)]\sin(\theta_b-\theta_{\rm in}). \tag{84}$$

Since $p_x''(t_1)>p_x''(t_0)$ and $\theta_b<\theta_{\rm in}$, we see that $\delta p_\parallel<0$. After a gyration, $p_\parallel$ always decreases. Hence, even if the x component of the particle velocity is slightly greater than the propagation speed of the small pulse,

$$v_{db}''\cos[(\pi/2)-\theta_b]+v_z''\cos\theta_b>v_{\rm sh2}, \tag{85}$$

the particle cannot easily take over the pulse. This suggests that some particles move with the small pulse for long periods of time.

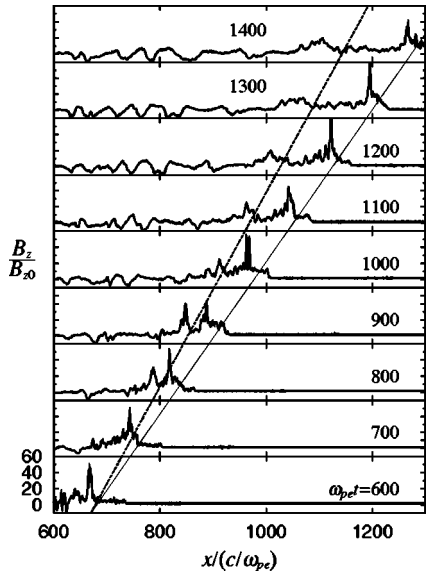

FIG. 4. Profiles of B_z at various times. The solid and dotted oblique lines indicate the trajectories of the shock front and the small pulse, respectively.

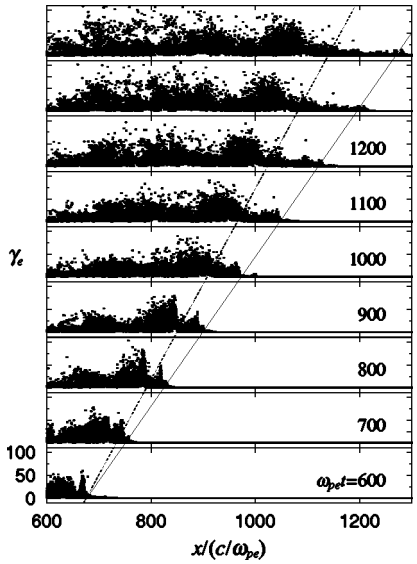

FIG. 5. Phase space plots (x, γ) of electrons. The solid and dotted oblique lines show the trajectories of the shock front and the small pulse, respectively. High-energy electrons are found behind the small pulse.

III. SIMULATIONS

We now study the present acceleration mechanism with one dimension (one space coordinate and three velocity components), relativistic, electromagnetic particle simulations.[19] We mainly discuss weak magnetic field cases, $|\Omega_e|/\omega_{pe}<1$.

The system length is $L=8192\Delta_g$, where Δ_g is the grid spacing. The number of simulation particles is $N_e=N_i=524\,288$. The ion-to-electron mass ratio is $m_i/m_e=100$; the thermal speeds are $v_{Ti}/(\omega_{pe}\Delta_g)=2.8\times10^{-2}$ and $v_{Te}/(\omega_{pe}\Delta_g)=0.28$. The electron skin depth is $c/\omega_{pe}=4\Delta_g$. The time step is $\omega_{pe}\Delta t=0.02$. The external magnetic field has x and z components, $\boldsymbol{B}_0=B_0(\cos\theta, 0, \sin\theta)$, and the waves propagate in the x direction (for more details of the method of shock simulation, see Refs. 1 and 20).

Figure 4 displays profiles of B_s of a shock wave. Here, the magnetic field strength is $|\Omega_e|/\omega_{pe}=0.4$ in the upstream region; accordingly, the Alfvén speed is $v_A/(\omega_{pe}/\Delta_g)=0.16$. The propagation angle is $\theta=60°$. The main pulse propagates with a speed $v_{sh}=18.8v_A$. The oblique straight line indicates the trajectory of the shock front; the cross points between this and horizontal lines show the x positions of the shock front. Behind the main pulse, we also find a small pulse propagating with a lower speed $v_{sh2}=15.0v_A$. The dotted line shows the trajectory of the small pulse. Figure 5 displays phase space plots (x, γ) of electrons. As in Fig. 4, the solid and dotted oblique lines show the trajectories of the shock front and small pulse, respectively. It is found that high-energy electrons are produced behind the small pulse. Their maximum energy is $\gamma\sim100$. Because the small-pulse speed is slightly lower than the speed of the main pulse, the region where high-energy electrons are generated slowly moves away from the shock front to the downstream region.

Figure 6 shows a snapshot of field profiles and electron phase space (x, γ) near the small pulse at $\omega_{pe}t=800$ (the main pulse is outside of these panels). The dotted vertical line indicates the x position of the maximum B_z in the small pulse; B_z and E_y have large values in the region $-5<(x-v_{sh2}t)/(c/\omega_{pe})<5$. Energetic electrons are present behind this pulse.

The top panel in Fig. 7 shows the time variation of $x-v_{sh2}t$ of an accelerated electron. For comparison, the time variation of an electron that was not accelerated is also depicted. The oscillations are due to the gyromotion in both cases; hence, the oscillation period of the nonaccelerated electron is much shorter than that of the accelerated one. The dotted horizontal line in the top panel indicates the position $(x-v_{sh2}t)/(c/\omega_{pe})=-5$; roughly, the rear edge of the small pulse. The accelerated particle stays around this position for a long time. The second panel shows $B_z[x(t)]$, where $x(t)$ is the position of the accelerated particle. The magnetic field is strong when the particle is above the dotted horizontal line in the top panel, i.e., when the particle is in the small-pulse region. The third panel shows the work W_σ done by the electric field E_σ, where $\sigma=x$, y, or z. The bottom panel

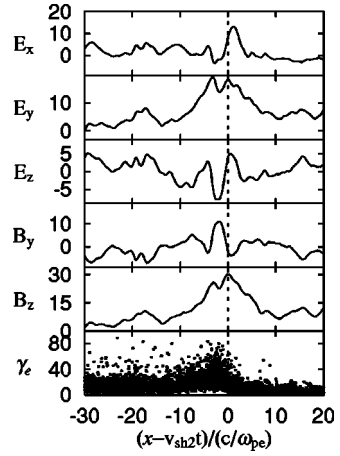

FIG. 6. Snapshot of field profiles and electron phase space (x, γ) near the small pulse at $\omega_{pe}t=800$. The field values are normalized to B_{z0}.

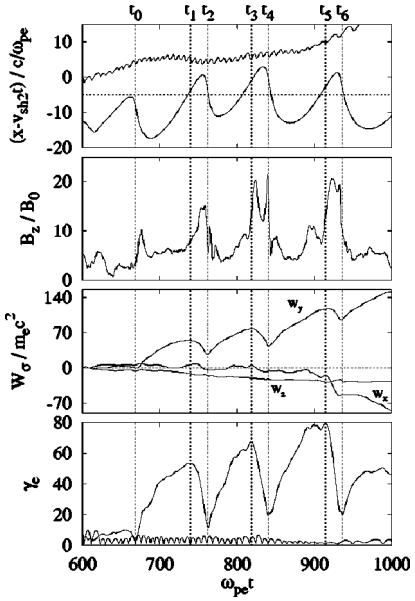

FIG. 7. Time variations of x, B_z, W_σ, and γ of an accelerated electron. The values of B_z are the ones at electron positions, and W_σ is the work done by the electric field E_σ ($\sigma=x$, y, or z). For comparison, the time variations of x and γ of a nonaccelerated electron are also plotted.

shows the time variations of γ; the lines with long- and short-period oscillations represent the accelerated and nonaccelerated particles, respectively. We find that W_y and γ of the accelerated particle have quite similar profiles. This indicates that the energy increase is mainly due to E_y, which is consistent with the physical picture presented in Sec. II. (For $\omega_{pe}t \gtrsim 950$, W_x goes down and the energy increase saturates. This is caused by the perturbation of E_x.) These panels clearly show that γ increases when the particle is in the downstream region while γ decreases when it is in the small pulse region.

The theoretical estimate of energy increase is of the same order of magnitude as the simulation result. The increase in γ from, for instance, time t_2 to t_3 is $\delta\gamma=55$. On the other hand, the theoretical estimate (83) gives the energy increase $\delta\gamma=57$ for the present simulation parameters. The average time rate of change of the maxima from time t_1 to t_5 is observed to be $\langle d\gamma/d(\omega_{pe}t)\rangle=0.15$, while Eq. (64) gives $\langle d\gamma/d(\omega_{pe}t)\rangle=0.2$ [where the field values observed in the simulation from t_2 to t_3 were substituted in Eq. (64)]. Also, $\langle d\gamma/d(\omega_{pe}t)\rangle$ for the minima is $\langle d\gamma/d(\omega_{pe}t)\rangle=0.065$ in the simulation, while Eq. (65) gives $\langle d\gamma/d(\omega_{pe}t)\rangle=0.04$.

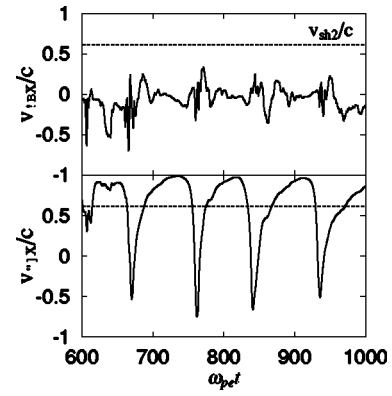

FIG. 8. Time variations of velocities $v_{\parallel x}$ and $v_{\perp x}$ of an accelerated electron.

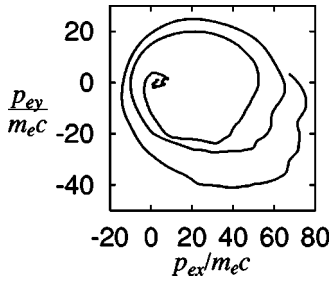

FIG. 9. Trajectory of the accelerated electron in the (p_x,p_y) plane.

Figure 8 shows the time variations of the x components of the parallel and perpendicular velocities of the accelerated electron; $v_{\parallel x}=(\boldsymbol{v}\cdot\boldsymbol{B})B_{x0}/B^2$ and $v_{\perp x}=[\boldsymbol{v}-(\boldsymbol{v}\cdot\boldsymbol{B})\boldsymbol{B}/B^2]\cdot\boldsymbol{e}_x$, where $\boldsymbol{e}_x$ is the unit vector in the x direction. The perpendicular velocity consists of gyration and drift velocities. The dotted horizontal lines indicate the propagation speed of the small pulse, $v_{sh2}=0.61c$. The velocity $v_{\parallel x}$ is much slower than v_{sh2}. The sum of the average values of $v_{\parallel x}$ and $v_{\perp x}$ is, however, close to the propagation speed of the small pulse; $\langle v_{\parallel x}\rangle+\langle v_{\perp x}\rangle \simeq v_{sh2}$, with $\langle v_{\parallel x}\rangle/c=-0.03$ and $\langle v_{\perp x}\rangle/c=0.64$.

Figure 9 shows the particle orbit projected on the (p_x,p_y) plane. As predicted by the theory, the orbit is ellipse type and its radius grows with time.

We now discuss parameter dependence of this acceleration. Figure 10 shows the maximum energy γ as a function of the Alfvén Mach number M_A for three different propagation angles; $\theta=45°$ (closed circles), $\theta=60°$ (white circles), and $\theta=80°$ (closed squares). The magnetic field strength is $|\Omega_e|/\omega_{pe}=0.3$, and hence the Alfvén speed is $v_A/(\omega_{pe}\Delta_g)=0.12$. The dotted vertical line indicates the shock speed $v_{sh}=c\cos\theta$ for $\theta=45$. Unlike the electron acceleration discussed by Bessho and Ohsawa,[1–3] the present acceleration mechanism is free from the condition $v_{sh}\sim c\cos\theta$.

Finally, we mention strong magnetic field cases, $|\Omega_e|/\omega_{pe}>1$. Figure 11 shows γ versus M_A for $|\Omega_e|/\omega_{pe}=2$ (closed triangles) and $|\Omega_e|/\omega_{pe}=3$ (white triangles). The propagation angle is $\theta=60°$. The left and right dotted vertical

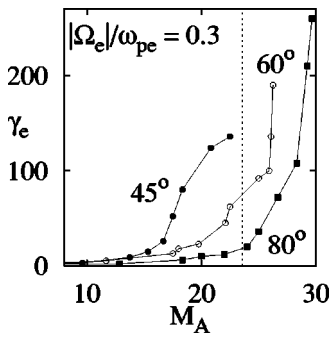

FIG. 10. Observed γ vs Alfvén Mach number M_A. The maximum energies observed in the simulations are plotted for three different propagation angles: $\theta=45°$ (closed circles), $\theta=60°$ (white circles), and $\theta=80°$ (closed squares). The frequency ratio is $|\Omega_e|/\omega_{pe}=0.3$. The dotted vertical line indicates the shock speed $v_{sh}=c\cos\theta$ for $\theta=45°$.

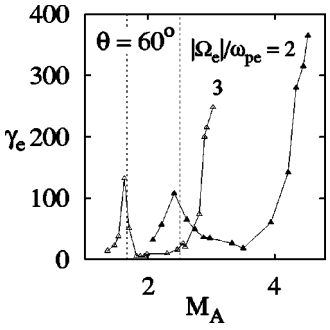

FIG. 11. Observed γ vs Alfvén Mach number M_A for strong magnetic field cases. The maximum energies for $|\Omega_e|/\omega_{pe}=2$ (closed triangles) and $|\Omega_e|/\omega_{pe}=3$ (white triangles) are plotted as functions of M_A. The propagation angle is $\theta=60°$. The left and right dotted vertical lines indicate the shock speed $v_{sh}=c\cos\theta$ for $|\Omega_e|/\omega_{pe}=3$ and $|\Omega_e|/\omega_{pe}=2$, respectively.

lines indicate M_A at which the condition $v_{sh}=c\cos\theta$ is satisfied for $|\Omega_e|/\omega_{pe}=3$ and $|\Omega_e|/\omega_{pe}=2$, respectively. For shock speeds with $v_{sh}\sim c\cos\theta$, strong acceleration occurs; it is due to the mechanism discussed by Bessho and Ohsawa.[1–3] For higher shock speeds, we also observe strong electron acceleration; this is due to the present mechanism.

IV. SUMMARY

With theory and particle simulations, we have found a new particle acceleration mechanism in shock waves. In this mechanism, electrons can be accelerated to ultrarelativistic energies in weak magnetic fields such that $|\Omega_e|/\omega_{pe}<1$ as well as in strong magnetic field $|\Omega_e|/\omega_{pe}>1$. The acceleration occurs in the vicinity of small pulses that are generated in a nonstationary large-amplitude shock wave. Because the propagation speeds of these small pulses are slightly lower than that of the main pulse, the acceleration region slowly moves away from the shock front to the downstream region.

We have analytically discussed the electron motion inside and outside such small pulses and obtained the amount of energy that electrons can gain from the wave field. With particle simulations, then, we have demonstrated the electron acceleration to energies $\gamma>100$ in both $|\Omega_e|/\omega_{pe}<1$ and $|\Omega_e|/\omega_{pe}>1$. The features of the accelerated electron motion in the simulations are consistent with the theoretical model.

Small pulses play an essential role in the present acceleration mechanism in large-amplitude shock waves. In the present simulation, the small pulse causing electron acceleration was generated by the ion reflection. The ion reflection gives rise to the oscillation of the shock amplitude, which then produces small pulses. Because the shock amplitude decreases with time owing to dissipation processes such as particle acceleration, small pulses generated at later times tend to have smaller amplitudes. Hence, the acceleration in those small pulses have not been observed. It is expected, however, that such pulses would be produced repeatedly in very large-amplitude shock waves such as supernova remnants or in large-amplitude magnetosonic waves in a turbulent plasma such as in solar flares. Also, it would be interesting to explore other mechanisms generating small pulses. As future work, it is important to study the properties of these pulses as well as to further investigate this acceleration mechanism.

ACKNOWLEDGMENT

This work was carried out by the joint research program of the Solar-Terrestrial Environment Laboratory, Nagoya University.

APPENDIX A: SIGN OF a_{in}^2

We show here that $a_{in}^2\geqslant 0$. Noting that

$$\gamma_{0in}\geqslant\gamma_{xz}, \tag{A1}$$

where

$$\gamma_{xz}=[1+(p_{x0}^2+p_z^2)/(m_e^2c^2)]^{1/2}, \tag{A2}$$

we find that

$$\frac{a_{in}^2}{\gamma_{din}^2}\geqslant m_e^2c^2\gamma_{xz}^2\gamma_{din}^2\left(1-\frac{v_{din}v_{x0}}{c^2}\right)^2-(m_e^2c^2+p_z^2). \tag{A3}$$

Substituting the relation

$$m_e^2c^2+p_z^2=m_e^2c^2(\gamma_{xz}^2-\gamma_{0in}^2v_{x0}^2/c^2)\leqslant m_e^2c^2\gamma_{xz}^2(1-v_{x0}^2/c^2) \tag{A4}$$

in Eq. (A3) yields

$$\frac{a_{in}^2}{\gamma_{din}^2}\geqslant m_e^2c^2\gamma_{xz}^2F(v_{x0}), \tag{A5}$$

where

$$F(v_{x0})=\gamma_{din}^2\left(1-\frac{v_{din}v_{x0}}{c^2}\right)^2-\left(1-\frac{v_{x0}^2}{c^2}\right). \tag{A6}$$

Its derivative is given as

$$\frac{dF}{dv_{x0}}=2\frac{\gamma_{din}^2}{c^2}(v_{x0}-v_{din}). \tag{A7}$$

We then see that $F(v_{x0})$ has its minimum value $F(v_{x0})=0$ at $v_{x0}=v_{din}$. Equation (A5) therefore indicates that $a_{in}^2\geqslant 0$.

APPENDIX B: ELLIPTIC MOTION FOR THE MAXIMUM ENERGY GAIN

Here, we show that accelerated electrons gain the maximum energy when $p_y(t_0)\sim p_y(t_1)\sim 0$. Also, we obtain the time periods t_1-t_0 and t_2-t_1.

We discuss electron motion in the frame moving with the velocity $\boldsymbol{v}_{db}$ relative to the laboratory frame. In this frame, the electric field vanishes behind the small pulse, $\boldsymbol{E}_b^*=0$, where the asterisk * denotes this frame, and the magnetic field is given as

$$\boldsymbol{B}_b^*=[0,0,\gamma_{db}(B_b-v_{db}E_b/c)]. \tag{B1}$$

Since there is no electric field, particles make circular motions; x^* and p_y^* may then be written as

$$x^*=-\frac{v_\perp^*}{\Omega_{eb}^*/\gamma^*}\sin\left(\frac{\Omega_{eb}^*}{\gamma^*}(t^*-t_0^*)\right)+x^*(t_0^*), \tag{B2}$$

$$p_y^* = -p_\perp^* \sin\left(\frac{\Omega_{eb}^*}{\gamma^*}(t^* - t_0^*)\right), \tag{B3}$$

for particles with $p_y^*(t_0^*)=0$, where Ω_{eb}^* is the nonrelativistic electron gyrofrequency,

$$\Omega_{eb}^* = -\frac{eB_b^*}{m_e c}, \tag{B4}$$

γ^* is the Lorentz factor of this particle. Also, $v_\perp^*$ and $p_\perp^*$ are the magnitudes of the velocity and momentum perpendicular to $\boldsymbol{B}_b^*$, respectively. The speed of the small pulse is given by

$$v_{\mathrm{sh2}}^* = \frac{v_{\mathrm{sh2}} - v_{db}}{1 - v_{db}v_{\mathrm{sh2}}/c^2}. \tag{B5}$$

Its rear boundary is then

$$x_r^* = v_{\mathrm{sh2}}^*(t^* - t_0^*) + x^*(t_0^*). \tag{B6}$$

One can obtain the time t_1^* from the equation $x^* = v_{\mathrm{sh2}}^*(t^* - t_0^*)$,

$$-\frac{v_\perp^*}{\Omega_{eb}^*/\gamma^*}\sin\left(\frac{\Omega_{eb}^*}{\gamma^*}(t^* - t_0^*)\right) = v_{\mathrm{sh2}}^*(t^* - t_0^*). \tag{B7}$$

Assuming the solution in the form

$$\frac{\Omega_{eb}^*}{\gamma^*}(t^* - t_0^*) = \pi + \frac{\Omega_{eb}^*}{\gamma^*}\delta t^*, \tag{B8}$$

where the time δt^* is much shorter than the gyroperiod,

$$\left|\frac{\Omega_{eb}^*}{\gamma^*}\delta t^*\right| < 1, \tag{B9}$$

we find that

$$\frac{\Omega_{eb}^*}{\gamma^*}\delta t^* \simeq \frac{\pi v_{\mathrm{sh2}}^*}{v_{\mathrm{sh2}}^* + v_\perp^*}. \tag{B10}$$

Since we consider relativistic particles, $v^* \sim c$, the assumption (B9) is satisfied. Substituting Eqs. (B8) and (B10) in Eq. (B3) yields p_y^* at $t^* = t_1^*$ when the particle reenters the small-pulse region

$$p_y^*(t_1^*) \simeq -p_\perp^* \frac{\pi v_{\mathrm{sh2}}^*}{v_{\mathrm{sh2}}^* + v_\perp^*}. \tag{B11}$$

This indicates that $p_y^*(t_1^*)=0$ when $v_{\mathrm{sh2}}^*=0$, i.e., when $v_{\mathrm{sh2}} = v_{db}$. Evidently, electrons gain the maximum energy when $p_y^*(t_1^*)=0$. We thus have $p_y(t_1)=0$.

Next, we obtain the laboratory time period $t_1 - t_0$ when the relation

$$\frac{\Omega_{eb}^*}{\gamma^*}(t_1^* - t_0^*) = \pi \tag{B12}$$

holds. From the Lorentz transformation of time

$$t_0 = \gamma_{db}(t_0^* - \boldsymbol{v}_{db}\cdot\boldsymbol{r}_0^*/c^2), \tag{B13}$$

and the equation $\boldsymbol{v}_{db}\cdot(\boldsymbol{r}_1^* - \boldsymbol{r}_0^*)=0$, it follows that

$$t_1 - t_0 = \gamma_{db}(t_1^* - t_0^*). \tag{B14}$$

With the aid of Eqs. (B1) and (B12), we find that

$$t_1 - t_0 = \gamma^*\gamma_{db}^2\frac{\pi}{|\Omega_{eb}|}, \tag{B15}$$

where

$$\gamma^* = \gamma_{db}\left(\gamma - \frac{\boldsymbol{v}_{db}}{c}\cdot\frac{\boldsymbol{p}(t_0)}{m_e c}\right). \tag{B16}$$

Similarly, we obtain the time period $t_2 - t_1$ as

$$t_2 - t_1 = \gamma^\dagger\gamma_{d\mathrm{in}}^2\frac{\pi}{|\Omega_{ein}|}, \tag{B17}$$

with

$$\gamma^\dagger = \gamma_{d\mathrm{in}}\left(\gamma - \frac{\boldsymbol{v}_{d\mathrm{in}}}{c}\cdot\frac{\boldsymbol{p}(t_1)}{m_e c}\right). \tag{B18}$$

For oblique waves, we also have the relations (B15)–(B18).

APPENDIX C: COMPARISON OF v_{db} AND $v_{d\mathrm{in}}$

We compare the magnitude of v_{db} and $v_{d\mathrm{in}}$. The small pulse is assumed to steadily propagate with a speed v_{sh2}. Hence, integrating the z component of Faraday's law in the region surrounding the rear boundary $x=x_r$, we obtain

$$\frac{v_{\mathrm{sh2}}}{c}(B_{\mathrm{in}} - B_b) = E_{\mathrm{in}} - E_b. \tag{C1}$$

We then find the relation

$$v_{db} - v_{d\mathrm{in}} = \frac{(B_{\mathrm{in}} - B_b)}{B_{\mathrm{in}}}(v_{db} - v_{\mathrm{sh2}}). \tag{C2}$$

Since $B_{\mathrm{in}} > B_b$, Eq. (C2) indicates that either Eq. (37) or Eq. (38) must hold. The former shows that v_{db} can become larger than $v_{d\mathrm{in}}$ when a small pulse propagates with a speed lower than the original large-amplitude pulse, which is the background of the small pulse.

Also, for oblique propagation where the magnetic field has the x component as well as the z components, the z component of Faraday's law gives

$$\frac{v_{\mathrm{sh2}}}{c}(B_{\mathrm{inz}} - B_{bz}) = E_{\mathrm{in}} - E_b. \tag{C3}$$

We therefore have the relations among the drift velocities and shock speed

$$v_{dbx} > v_{d\mathrm{in}x} > v_{\mathrm{sh2}} \tag{C4}$$

or

$$v_{dbx} < v_{d\mathrm{in}x} < v_{\mathrm{sh2}}, \tag{C5}$$

where $v_{dbx} = cE_bB_{bz}/B_b$ and $v_{d\mathrm{in}x} = cE_{\mathrm{in}}B_{\mathrm{inz}}/B_{\mathrm{in}}$.

[1] N. Bessho and Y. Ohsawa, Phys. Plasmas **6**, 3076 (1999).
[2] N. Bessho and Y. Ohsawa, Phys. Plasmas **7**, 4004 (2000).
[3] N. Bessho and Y. Ohsawa, Phys. Plasmas **9**, 979 (2002).
[4] D. J. Forrest and E. L. Chupp, Nature (London) **305**, 291 (1983).
[5] S. R. Kane, E. L. Chupp, D. J. Forrest, G. H. Share, and E. Rieger, Astrophys. J. Lett. **300**, L95 (1986).
[6] T. Tanimori, K. Sakurazawa, S. A. Dazeley *et al.*, Astrophys. J. Lett. **492**, L33 (1998).

[7]F. A. Aharonian, A. G. Akhperjanian, J. A. Barrio *et al.*, Astrophys. J. **539**, 317 (2000).
[8]K. Koyama, R. Petre, E. V. Gotthelf *et al.*, Nature (London) **378**, 255 (1995).
[9]T. Tanimori, Y. Hayami, S. Kamei *et al.*, Astrophys. J. Lett. **497**, L25 (1998).
[10]J. H. Adlam and J. E. Allen, Philos. Mag., Suppl. **3**, 448 (1958).
[11]L. Davis, R. Lüst, and A. Schlüter, Z. Naturforsch. A **13**, 916 (1958).
[12]Y. Ohsawa, Phys. Fluids **29**, 2474 (1986).
[13]C. S. Gardner and G. K. Morikawa, Commun. Pure Appl. Math. **18**, 35 (1965).
[14]T. Kakutani, H. Ono, T. Taniuti, and C. C. Wei, J. Phys. Soc. Jpn. **24**, 1159 (1968).
[15]Y. Ohsawa, Phys. Fluids **29**, 1844 (1986).
[16]B. Lembege and P. Savoini, J. Geophys. Res. [Space Phys.] **107** (2002).
[17]T. Kawashima, S. Miyahara, and Y. Ohsawa, J. Phys. Soc. Jpn. **72**, 1664 (2003).
[18]S. Usami and Y. Ohsawa, Phys. Plasmas **11**, 918 (2004).
[19]P. C. Liewer, A. T. Lin, J. M. Dawson, and M. Z. Caponi, Phys. Fluids **24**, 1364 (1981).
[20]Y. Ohsawa, Phys. Fluids **28**, 2130 (1985).